ELSEVIER

Polymer 43 (2002) 6751–6760

polymer

www.elsevier.com/locate/polymer

Limited-supply diffusion in the liquid polystyrene–glassy poly(phenylene oxide) pair. Further results in extended times scale

J. Pablo Tomba[a], José M. Carella[a,*], José M. Pastor[b,c], Juan C. Merino[c]

[a]*Instituto de Investigaciones en Ciencia y Tecnología de Materiales, (INTEMA) (UNMdP-CONICET), Facultad de Ingeniería, Universidad Nacional de Mar del Plata, Juan B. Justo 4302, 7600 Mar del Plata, Argentina*

[b]*Departamento de Física de la Materia Condensada, Escuela Técnica Superior de Ingenieros Industriales, Universidad de Valladolid, Paseo del Cauce s/n 47011, Valladolid, Spain*

[c]*Centro de Investigación y Desarrollo en Automoción (CIDAUT), Parque Tecnológico de Boecillo, Parcela 209, 47151 Valladolid, Spain*

Received 4 March 2002; received in revised form 26 August 2002; accepted 29 August 2002

Abstract

Diffusion between a liquid polystyrene and a glassy poly(phenylene oxide) matrix is experimentally studied over a wide range of temperatures and diffusion times, using confocal Raman microspectroscopy. A specially designed experimental setup allows precise direct following of time evolution of the chemical composition profiles along the diffusion path. A direct and precise quantification is made for the experimental errors involved in two methods used for Raman measurements. An already proposed diffusion model is used to predict the time evolution of the advancing composition profiles along the diffusion path, and gives precise results. Experimental thermodynamic and kinetic data taken from literature are used for the model calculations, and excellent agreement with experimental results is obtained. Diffusion slow down is confirmed at the lowest diffusion temperature used, and probable causes are discussed.

Keywords: Limited-supply diffusion; Physical properties; Polystyrene

1. Introduction

Diffusion between low and high molecular weight liquids, and amorphous polymer matrices in the glassy state, has received considerable attention in recent years. For the general case of polymer–polymer diffusion, two concentration regimes may be distinguished. Diffusion of species in the dilute regime does not change appreciably the matrix physical properties along the diffusion path, and calculations can be done via an 'independent' diffusion coefficient for each component [1]. Diffusion in concentrated regime deserves special attention, because many physical properties of the local environment are very different from those of the diffusing species, and the diffusion process produces changes in most of the matrix physical properties [2]. This article addresses only diffusion processes in the concentrated regime.

Because of the above mentioned characteristics, the penetration of small molecules into structural parts in service may seriously affect their properties and durability. Many examples can be found in the automotive market (as in the case of 'under the hood' parts which are exposed to vapor and liquid hydrocarbons). Extension of the studies to diffusion of larger liquid molecules follows naturally, both to encompass the wide range of molecular sizes of organic molecules that may be put in contact with parts in service, and to verify and validate proposed diffusion mechanisms.

Many articles have addressed the subject of diffusion of small penetrant molecules (solvent and non-solvent) into glassy matrices over wide range of concentration and temperature [3–14]. Several types of diffusion mechanisms have been described and characterized, and also some have been modeled [3–6,10]. A thorough description of the mechanisms involved in the diffusion processes of small molecules into glassy polymeric matrices (including an enlightening discussion on the osmotic pressure meaning and effects) can be found in Ref. [10].

Several features are observed only for this special case of diffusion of small molecules in the concentrated range.

* Corresponding author.
E-mail address: jcarella@fi.mdp.edu.ar (J.M. Carella).

0032-3861/02/$ - see front matter
PII: S0032-3861(02)00634-1

Mass transport into the glassy matrix, associated with a sharp composition profile diffusion front with a small Fickian tail ahead of it, is controlled by the swelling rate of the glassy matrix just ahead of the diffusion front, which is proportional to a high positive power of the osmotic pressure [8]. For the glassy matrix to be swollen and extruded, the local osmotic pressure must overcome the local matrix yield stress [4–8]. For diffusion experiments where the supply of small penetrant molecules is unlimited, the temperature dependent penetration rate of the established diffusion front is a constant. The presence of the Fickian tail ahead of the diffusion front that advances, and its constant advancing rate for the case of unlimited supply of small penetrant molecules are the most often cited characteristics of the diffusion mechanism known as Case-II.

Small molecules are associated with large osmotic pressure values [10], and therefore they can penetrate polymeric glassy matrices even in those cases where the Flory thermodynamic interaction parameter may be unfavorable. Larger liquid molecules are associated with much smaller osmotic pressure values, and therefore these must be miscible with the glassy matrix in order to be able to dissolve and plasticize the matrix. Miscibility is always associated with favorable Flory thermodynamic interaction parameter values. Therefore, immiscible small molecules may penetrate polymeric glassy matrices without dissolving the polymer—via Case-II diffusion mechanism—and for unlimited supply of liquid an equilibrium state will be eventually reached, with a swollen polymer in contact with pure non-miscible liquid. On the other hand, if the liquid is miscible with the polymeric glassy matrix it will dissolve the matrix, and the final equilibrium state will be a homogeneous solution; during the transient diffusion process the glassy matrix may be penetrated by a Fickian tail whose size depends heavily on the liquid osmotic pressure. Cross-linked polymers are obviously excluded from this discussion.

A complete description of a proposed diffusion mechanism for liquid large molecules into miscible glassy polymeric matrices has been published recently [15]. As the osmotic pressure associated with large liquid molecules is extremely low, it is assumed that: (a) the glassy matrix is dissolved relatively rapidly at the interface, and (b) a relatively slow liquid–liquid diffusion process is controlled mainly by the local T_g. In Ref. [15], the most important features of the diffusion of small molecules into glassy polymeric matrices are also described, paying careful attention to the most relevant experimental and modeling results published. The influence of the liquid molecular size on the osmotic pressure is pointed out, and the controlling diffusion process for large molecules is modeled for the whole diffusion path in the liquid, based on the effects of the Flory thermodynamic interaction parameter, local molecular weight distribution, local glass transition temperature values (Local T_g), composition dependent monomeric friction coefficient, and diffusion temperature. As a direct consequence of the huge changes of the molecular mobility caused by the changes in the local T_g along the diffusion path: (1) the composition profile shows a sharp diffusion front without a Fickian tail ahead, and (2) for the case of unlimited liquid supply, the temperature dependent penetration rate is not a constant but decreases with the penetration length. These two features are not observed in the diffusion of small molecules into glassy matrices. Experimental results for diffusion of liquid polystyrene (PS) into glassy poly(phenylene oxide) (PPO) are also used to verify the proposed model predictions.

Some published experimental results dealing with diffusion of large liquid molecules into glassy matrices [11–13] are also analyzed in the above mentioned article. It is suggested that all these diffusion processes of large liquid molecules can be interpreted in terms of the above mentioned model.

Also, experimental results for diffusion of large plasticizer molecules (RDP) into a glassy ULTEM matrix [14] were analyzed. It was observed that the main characteristics reported for the RDP-ULTEM limited-supply diffusion experiments qualitatively coincide with predictions of the diffusion model proposed in Ref. [15], which is different from Case-II diffusion: (a) sharp diffusion fronts, (b) RDP concentration at the outer layer constantly decreasing with time, (c) no diffusion at temperatures below the matrix T_g, (d) changes of advancing front velocities similar to the model predictions, (e) uncertainty about the existence of Fickian tails ahead of the advancing diffusion front. Because of the lack of experimental data on RDP-ULTEM monomeric friction coefficient and Flory thermodynamic interaction parameter, the advancing diffusion front velocities time changes at several temperatures were qualitatively compared with the model predictions for the behavior of the PS–PPO system. Within the large experimental errors of the data reported in Ref. [14], the agreement was good. Both this qualitative agreement and the large size of the RDP molecule led to suggest that the RDP osmotic pressure at the RDP-ULTEM interface ought to be very low, and therefore the diffusion mechanism may not be Case-II.

Nevertheless, in a recently published work on diffusion of the same RDP-ULTEM system, improved experimental results were presented for unlimited RDP supply [16]. These results were obtained via a much better experimental design that eliminates the RDP losses present in the limited-supply experiments, which was the main cause of experimental error. Constant (temperature dependent) penetration rates and observation of Fickian tails ahead of the penetration front are reported [16]. Even while the large RDP molecular size can be associated with low osmotic pressure values, its diffusion into the ULTEM matrix seems to follow the Case-II mechanism and suggests that a transition regime may exist for diffusion of some large molecules into miscible glassy matrices.

The diffusion of liquid PS into glassy PPO has been used

as a model system to verify the diffusion mechanism proposed in Ref. [15], with excellent results; it was chosen mainly on the basis of unlimited miscibility and large volume size for the PS molecules, and the availability of thermodynamic and kinetic data in the open literature. In view of the above discussion on the RDP-ULTEM diffusion results, two facts must be pointed out:

1. For all PS–PPO experiments it was observed that the penetration rate of the diffusion front depends markedly on WLF parameters, on the Flory thermodynamic interaction parameter, on local T_g values and on the monomeric friction coefficient values. As the experimental data on thermodynamic interaction parameter and on monomeric friction coefficient values used for the model simulations were taken from other authors work, small experimental errors may be magnified by the model simulations.
2. The PS volume fraction versus diffusion coordinate profiles used to verify the diffusion model predictions were measured for some temperatures and sparse diffusion times, using one sample for each measurement. Since there is always a small random error associated with the measurement of the initial thin (PS-rich) layer thickness, this fact may also contribute to random experimental error.

The fact that we can always suspect a small random error in the measurement of the initial thin (PS-rich) layer thickness—and this may have an effect on the quantitative measurement of the diffusion front advancing velocities—suggests the convenience of quantitatively verifying the predictions of the model proposed in Ref. [15], and the accuracy of the parameters involved in the diffusion model predictions. For this purpose, limited-supply diffusion experiments, conducted for shorter and longer times on the PS–PPO system, with frequent periodic measurements on the same spot of the same sample, were performed over an extended temperature range. The use of the same spot of the same sample eliminates the random error associated with the measurements of the initial thin layer thickness. The same set of experiments is also used to verify the anomalous behavior observed for the diffusion experiments conducted previously at 100 °C [15].

2. Experimental

Two types of miscible polymers were used for the experiments: polystyrene (PS) and poly(phenylene oxide) (PPO). Anionically polymerized polystyrene (PS740, $\bar{M}_w$ = 740 g/mol, $\bar{M}_n$ = 700 g/mol) was purchased from Polymer Source (Dorval, Canada). The PPO sample used ($\bar{M}_w$ = 31 000 g/mol, $\bar{M}_n$ = 15 500 g/mol) was provided by General Electric. Molecular weight characterization details were provided by the makers. All samples were exhaustively dried under vacuum before using, to remove any traces of solvent or moisture present, because small amounts of solvents can change the T_g and affect the diffusion rate.

Two homogeneous blends were prepared by weighing the polymers in the desired proportions, dissolving the solids in benzene at room temperature (about 10% (w/w) solutions), and freeze-drying the necessary amounts of solutions. The high-T_g blend is made out of 95/5 (w/w) PPO/PS. The low-T_g blend is made out of 30/70 (w/w) PPO/PS.

Glass transition temperatures (T_g) for pure polymers and homogeneous blends were determined by differential scanning calorimetry (DSC), using a Perkin–Elmer Pyris II DSC. Reported T_g values were always calculated as the onset of the thermal transition. The high-T_g blend shows a transition at 473 K; the low-T_g blend shows a transition at 298 K.

A generalized Fox-type equation has been used in previous works to correlate the blend composition dependence on the blend T_g [17]. For this work a low-degree polynomial form has been used, for the sake of better accuracy and simplicity when used in calculations.

Slender composite plates were prepared as described elsewhere [18]. For each composite plate, a thick layer (about 500 μm thick) was prepared by vacuum molding a weighted amount of the high-T_g blend, at temperatures at least 20 K above the blend T_g. A thinner layer (typically between 40 and 80 μm thick) of the low-T_g blend was then vacuum molded on top of the thick layer, at temperatures conveniently chosen below the thick layer T_g, to minimize diffusion at this stage. Precisely machined and polished cylindrical molds were used for each of the molding stages. The molds consist of hollow cylinders with sliding pistons, which are connected to a vacuum pump. The sliding pistons ends were machined in a precision lathe, and carefully polished to achieve an optically flat surface. The freeze-dried blends (both high and low-T_g) were placed in the mold as solids; then the mold was connected to a vacuum pump to reduce the air pressure below 10^{-4} MPa, and then the whole mold temperature was raised to the values desired for each molding operation. Before conducting the diffusion experiments, the PS volume fraction for many points along the diffusion coordinate were measured for all the samples used, as explained later; this was done to check for any amount of diffusion that might have occurred during the molding stage. Adequate corrections were made on the calculations of the diffusion process, based on these measurements.

Diffusion between layers of the composite plates was promoted by elevating the temperature in a controlled oven (±0.5 K) for specified period of time. The oven was continuously flushed with dry nitrogen gas, to avoid sample oxidation. The samples were periodically removed from the

Table 1
Thin layer thickness, and diffusion conditions for all experiments

Sample	Thin layer thickness (±5 μm)	Total diffusion time (h)	Number of time periods	Diffusion temperature (±0.5 K)
A	55	214	11	373
B	65	227	10	393
C	85	40	11	393
D	60	150	11	413
E	70	98	10	433

oven after each time period, and allowed to quickly cool down to room temperature before Raman measurements (Table 1). The composite plates were molded into specially designed holders, which allow a precise placement of the Raman laser beam, always within ±10 μm of the same spot at the sample surface.

Local Raman spectra for pure PPO, pure PS and blends were measured at room temperature, on a Raman Microspectrometer DILOR LabRam Confocal, using a 16 mW He–Ne laser beam. Slit opening used was 500 μm, with a pinhole opening of 100 μm and a holographic grating of 1800 lines/mm, which allows acquiring data in a frequency range between 500 and 1500 cm^{-1}. Usually 10 spectra were accumulated for each data point, and the total acquisition time for each data point was 300 s. The characteristic Raman bands used for calculations are located in this frequency range.

Local chemical composition for many points along the diffusion coordinate had to be calculated from Raman spectroscopy data. Two focusing methods can be used [19], and each one has advantages and drawbacks:

(a) In the procedure named as Method A in Ref. [19], the laser beam is aligned in a direction perpendicular to the diffusion direction. The errors caused by instrumental effects are minimized, but the sample has to be cut and microtomed, and therefore each sample can be used to study the results for one diffusion time only.
(b) If the procedure named as Method B in Ref. [19] is used, the laser beam is aligned in a direction parallel to the diffusion coordinate and focused deeper into the sample, without cutting or microtoming. Some instrumental effects have to be corrected to obtain precise results, but a large number of measurements—for many diffusion times—can be made without altering the sample. This procedure eliminates uncertainties about experimental errors in the samples manufacture, and this feature makes it preferred for this work.

Because of the need to make a large number of measurements on the same spot of the same sample—to minimize errors—the laser beam was always aligned in a direction parallel to the diffusion coordinate, and the instrumental effects were calculated and corrected, as explained below. A few experiments were also done, for selected temperatures and diffusion times, where both types of measurement methods were used for the same sample: composition profiles were first measured using Method B, and then the samples were cut and microtomed to measure composition profiles by Method A. We have labeled these experiments as Double-Method Samples, and used them to check the accuracy of the corrections applied for instrumental effects.

When the measuring Method B is used (laser beam aligned parallel to the diffusion coordinate) two separate instrumental effects have to be considered and corrected.

(a) The laser beam of the Confocal Raman Microspectrometer is refracted when it travels trough an air–polymer interface. Therefore, when traveling deeper from the polymer surface the real focus is placed deeper than the micrometric positioning screw indication, and this geometric effect increases linearly with depth. The effect has been described and modeled in a recent publication [20], and the results presented at this article have all been corrected for this effect.
(b) Confocal Raman Microspectrometers show a characteristic bell-shaped spatial resolution curve in both directions parallel to the laser beam axis. When the laser beam is focused perpendicular to a flat microtomed surface—not deeper than 5 μm—the instrumental resolution—expressed as the full width at half maximum of the resolution curve, (FWHM)—is 2.5 μm. This fact is a constant along the whole diffusion coordinate when Method A is used, and therefore no correction for this effect is needed for the purpose of this work [21]. When the laser beam is focused parallel to the diffusion coordinate, starting from the surface to depths of up to 200 μm (Method B), the instrumental resolution becomes much poorer (the deeper the poorer). Recently published work demonstrates that the FWHM for the depth resolution curve increases with focusing depth; also a model for this depth-dependent FWHM is presented [20].

For this study, these effects are taken into account when comparing the diffusion model predictions with the experimentally measured PS volume fractions versus diffusion distance profiles. Details of the methods used can be found elsewhere [22].

Local Raman spectra were measured along the diffusion

coordinate, aligning the laser beam in a direction parallel to the diffusion coordinate. Many spectra were acquired, focusing the laser beam at different depths along the diffusion path, in steps of 2–5 μm (typically 30–40 points along the diffusion path). Local chemical compositions were calculated from the acquired local Raman spectra, using a linear decomposition method [23].

Five samples were used for the whole set of diffusion experiments, as detailed in Table 1. Four different diffusion temperatures were used, and the number of diffusion time periods and the total diffusion time are also shown in Table 1. A few experiments were performed to verify the composition profiles distortions caused by the above mentioned instrumental effects. For three different samples, diffusion was allowed to proceed at 393K so that the interphases are placed between 50 and 100 μm deep. For these three samples, composition profiles were measured by two different methods: (a) the laser beam was aligned parallel to the diffusion coordinate, and local spectra were measured focusing the Raman laser deeper starting from the sample surface, (b) the samples were fractured along a surface parallel to the diffusion coordinate, and this surface was microtomed flat; Raman spectra were measured aligning the laser beam perpendicular to the microtomed surface and to the diffusion coordinate. The method (a) is affected by the instrumental effects, while method (b) is not.

3. Physical diffusion model used

The interdiffusion process between PS and PPO, each one with a given distribution of degrees of polymerization ($l_1^{PS} \le l^{PS} \le l_2^{PS}$) and ($l_1^{PPO} \le l^{PPO} \le l_2^{PPO}$) can be described by the following set of diffusion equations [2,17,24]:

$$\frac{\partial \Phi_l^{PS}}{\partial t} = \vec{\nabla}(\Lambda_l^{PS} \nabla \mu_l^{PS}) + \vec{\nabla}(\Phi_l^{PS} \vec{J}_v) \tag{1a}$$

$$\frac{\partial \Phi_l^{PPO}}{\partial t} = \vec{\nabla}(\Lambda_l^{PPO} \nabla \mu_l^{PPO}) + \vec{\nabla}(\Phi_l^{PPO} \vec{J}_v) \tag{1b}$$

In Eqs. (1) Φ_l^i, μ_l^i and Λ_l^i are the concentration (volume fraction), chemical potential and diffusivity (Onsager coefficients) of i polymer with polymerization degree l, respectively. The bulk flow $\vec{J}_v$ is defined by

$$\vec{J}_v = \vec{J}^{PS} + \vec{J}^{PPO} \tag{2}$$

where

$$\vec{J}^i = -\sum_{l=l_1^i}^{l_2^i} \Lambda_l^i \vec{\nabla} \mu_l^i \tag{3}$$

The system of Equations (1) is required to satisfy the following restriction, at every point along the diffusion coordinate:

$$\sum_l \Phi_l^{PS} + \sum_l \Phi_l^{PPO} = 1 \tag{4}$$

This simple mass conservation equation is equivalent—at the liquid PS–glassy PPO interface—to a dissolution velocity much faster than the diffusion process, as provides PPO to the liquid layer without other limit than the established by the diffusion equations.

As the PS used is a nearly monodisperse component, and it is also the diffusion controlling species, the general scheme presented in Ref. [15] can be simplified considering a diffusion process with two-components: PS and PPO with polymerization degrees l^{PS} and l^{PPO}, respectively. Assuming monodisperse components, the diffusion process can be modeled using a single binary diffusion coefficient [24]

$$D = kT(\Phi^{PPO}\Lambda^{PS} + \Phi^{PS}\Lambda^{PPO}) \times \left[\frac{\Phi^{PS}}{l^{PPO}} + \frac{\Phi^{PPO}}{l^{PS}} - 2\chi\Phi^{PS}\Phi^{PPO} \right] \tag{5}$$

where the chemical potentials have been derived form the Flory–Huggins theory for monodisperse systems [24].

In the range of blend composition selected for this work, the PS sample used has an average molecular weight smaller than the entanglement molecular weights of the blends. For this reason Rouse dynamics is assumed for the PS species. In this case, the Onsager coefficient for PS becomes [2,24]

$$\Lambda^{PS} = \frac{1}{\zeta_0^{PS}} \Phi^{PS} \tag{6}$$

where ζ_0^{PS} is the monomeric friction factor for the PS species.

Experimental values of the monomeric friction factors for PS and PPO as a function of blend composition—corrected at a constant $(T - T_{g,blend})$ values—were taken from Fig. 4 of Ref. [25]. For the calculations, the composition dependences of the monomeric friction factors—at constant $(T - T_{g,blend}) = 3$ K—have been fitted in terms of the PS volume fraction using the following expressions

$$\log \zeta_0^{PS} = 0.341 + 6.403\Phi^{PS} - 4.686(\Phi^{PS})^2 \tag{7}$$

$$\log \zeta_0^{PPO} = 4.745 + 0.104\Phi^{PS} - 1.104(\Phi^{PS})^2 \tag{8}$$

where the units for ζ_0 are (dyn s/cm).

The WLF equation used to model the strong dependence of friction factors on T and on the local T_g ($T_{g,blend}$) is [25,26]

$$\log \frac{\zeta_0(T_{ref})}{\zeta_0(T)} = \frac{-12.5(T - T_{ref})}{48.9 + T - T_{ref}} \tag{9}$$

where $T_{ref} = T_{g,blend} + 3$ K.

A low-degree polynomial was used to correlate very precisely the blend composition dependence of the blend T_g. The polynomial used in the calculations has the form

$$T_{g,blend} = 483.73 - 412.29\Phi^{PS} + 206.68(\Phi^{PS})^2 \tag{10}$$

where the unit for $T_{g,blend}$ is (K).

Values of the Flory thermodynamic interaction

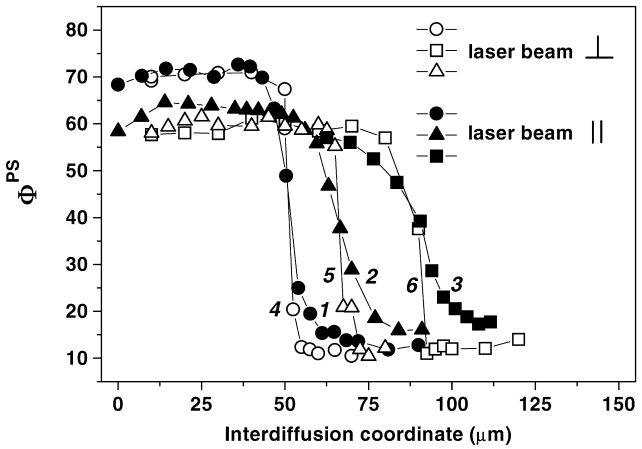

Fig. 1. Experimental PS volume fractions profiles for the Double-Method Samples. Open symbols: Method A (laser aligned perpendicular to the diffusion coordinate). Solid symbols: Method B (laser aligned parallel to the diffusion coordinate).

parameter (χ) for the dPS–PPO polymer pair can be found in Ref. [26]. The authors have reported values of the χ parameter independent of local blends composition, dependent only on temperature. The temperature dependence found for the χ parameter—in the range of temperature between 454 and 588 K—is given by

$$\chi = 0.112 - \frac{62.0}{T} \tag{11}$$

where T is the absolute temperature (K). The relative importance of the entropic and enthalpic terms on the calculation of the chemical potential gradients have been thoroughly discussed in Ref. [15].

A finite elements scheme was used to solve the systems of Equations (1), as detailed in Ref. [17]. The restriction imposed by Eq. (4) has been explicitly included in the calculation scheme using a Lagrange multipliers strategy. Non-flux or Newmann boundary conditions are used at the outer surfaces of the sample.

4. Results and discussion

Fig. 1 shows the measured values for PS volume fractions versus interdiffusion coordinate for the three Double-Method Samples used to verify the composition profiles distortions caused by the confocal Raman instrumental effects. The curves 1–3 were measured first—as described in Section 2—using Method B: the laser beam was aligned parallel to the diffusion coordinate, and successive measurements were done, each time focusing deeper away from the surface, from about 5 to 120 μm. For curves 1–3, the focusing depth was corrected as mentioned before, applying the method proposed in Ref. [20]. The refraction indexes used are 1.59 for both PS and PPO. The curves 4–6 were measured later, after cutting the samples and microtoming flat on a plane parallel to the diffusion coordinate, as described earlier (Method A in Ref. [19]). For Method A the laser beam is aligned perpendicular to the diffusion coordinate.

All the composition profiles show the expected shapes for limited-supply diffusion between layers with different chemical composition and glass transition temperatures. Two plateau regions are connected by a narrow interphase along which the local chemical composition changes rapidly.

Comparing curves 1–3 and curves 4–6, the effect of the instrumental resolution FWHM enlargement can be clearly seen when traveling deeper along the diffusion coordinate.

Four important points must be mentioned after observing Fig. 1:

1. For the regions where the blend compositions do not change along the diffusion coordinate, results obtained using Methods A and B coincide within experimental error. This is expected for the causes above mentioned for the instrumental errors present in Method B, because lower slopes in the composition profiles will be much less affected by the enlargement of the depth range over which the Raman signal is effectively averaged [20].
2. Looking at curves 1–3—in this order—we can observe that the interphase regions width seem to grow wider the deeper they are measured by Method B, while Method A measurements indicate that the interphase is much narrower and the broadening observed for curves 1–3 is an instrumental artifact. The cause of the interphase broadening is clearly the enlargement of the depth range over which the Raman signal is effectively averaged (FWHM increase). This interphase width enlargement can be seen in Fig. 1 as a decreasing of the highest curves slopes.
3. Assuming that within the small interphase width the instrumental resolution (FWHM) does not change appreciably, the middle-points of the highest slopes are taken as references for the depth corrections used [20]. It can be observed that the depth correction is precise and makes the corrected curves 1–3 middle-points to coincide precisely with the middle-points of curves 4–6. The same correction procedure has been used for experiments where no diffusion is involved at the interface, with similar results.
4. The same effect mentioned in point (3)—poorer instrumental resolution due to the FWHM enlargement—is responsible for the fictitious tails observed in curves 1–3—ahead and behind the diffusion front—which are not present in curves 4–6 because of the much better instrumental resolution obtained with the Method A. The fictitious tails are more pronounced for interphases placed deeper from the surface (further away form the abscissa origin), as expected because of the increase of FWHM with the focusing depth increase.

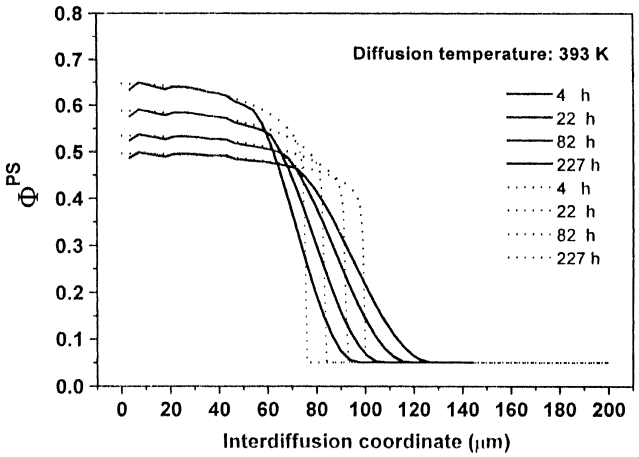

Fig. 2. Diffusion model simulations for the PS volume fractions profiles for the diffusion experiment conducted at 393 K (Sample B in Table 1). Dotted lines: raw model predictions. Solid lines: model prediction convoluted with the bell-shaped instrumental depth resolution curve.

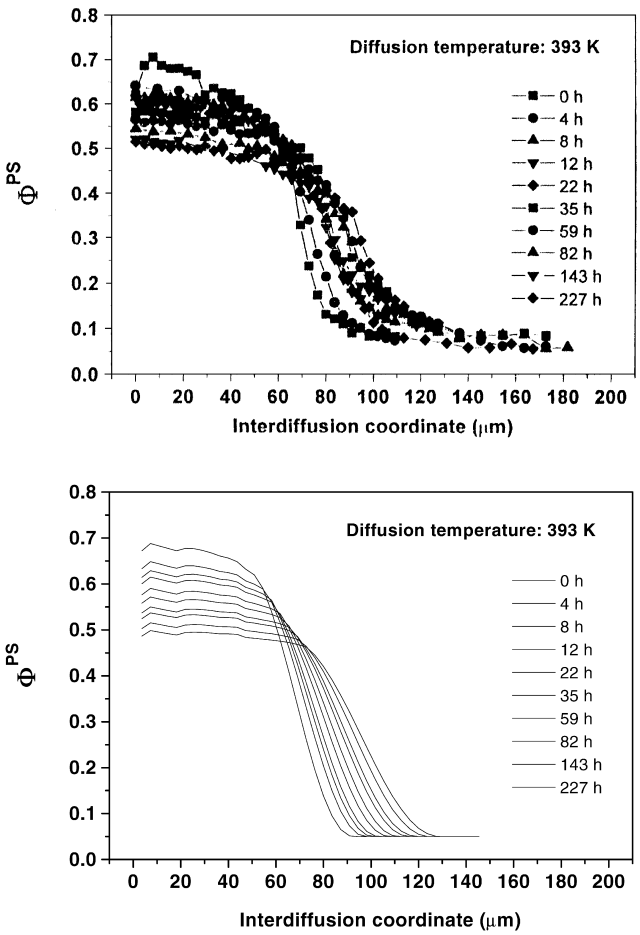

Fig. 3. (A) Experimental PS volume fractions profiles for the diffusion experiment conducted at 393 K (Sample C in Table 1). Measurements were made using the Method B (laser aligned parallel to the diffusion coordinate). (B) Convoluted diffusion model simulations for the PS volume fractions profiles for the diffusion experiment conducted at 393 K (Sample B in Table 1).

Every other composition profiles measured for the other samples used for this work have been obtained using Method B; the focusing depths have been always corrected as described in Ref. [20], and the fictitious tails observed ahead and behind the diffusion front are disregarded for comparison with the diffusion model predictions.

Fig. 2 shows simulated results for the diffusion experiments. The simulations were performed solving Eq. (1a) for the PS component subjected to the mass conservation law given by Eq. (4). A single binary diffusion coefficient given by Eq. (5) was used. Eqs. (7–9) were used to model the composition and temperature dependence of the monomeric friction factor for PS and PPO components. The composition dependence of blend T_g was fitted using Eq. (10). Values of Flory thermodynamic interaction parameter were calculated for each temperature using Eq. (11).

Results predicted by the diffusion model used for several diffusion times at 393 K are shown in Fig. 2 as dotted lines. All the characteristics expected for this type of diffusion experiments are observed: The highest slope region, associated with a higher T_g is located next to the glassy matrix, and a gradually decreasing slope shows the influence of the local T_g profile that rapidly decreases along the PPO diffusion path, thus quickly causing a chemical composition plateau. No tails are predicted by the model ahead of the diffusion front, and this result ought to be expected from the model formulation assumptions. The limited PS supply causes the PS concentration at the outer layer to decrease with diffusion time, and the very narrow interphase advances maintaining an almost square-box shape for the PS concentration profile.

In order to compare the diffusion model predictions with the experimental measurements, the instrumental effects present in Method B were also simulated. The effect of the confocal Raman depth resolution was simulated by convoluting the diffusion model predictions—shown in Fig. 2 as dotted lines—with the bell-shaped instrumental resolution curve proposed in Ref. [20], that depends on the focusing depth. The convoluted profiles are shown in Fig. 2 as solid lines. The diffusion model predictions (dotted lines) show the same characteristics as the composition profiles measured by Method A, shown in Fig. 1. The convoluted profiles show the same characteristics as the composition profiles measured by Method B, shown in Fig. 1. Later, simulations results will be quantitatively compared with experimental data.

Experimental results obtained for diffusion at 393 K are shown in Fig. 3A. The PS concentration profiles were measured for several diffusion times, using the Method B, always for the same spot of the same sample. The curves show the same characteristics as the convoluted profiles shown in Fig. 2 as continuous lines. The influence of the focusing depth on the instrumental resolution causes the gradual decrease of the slope measured at the interphase, and the increased size of the fictitious tails ahead and behind

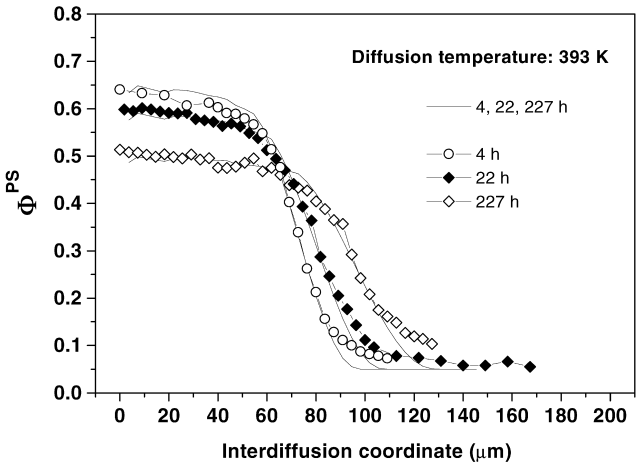

Fig. 4. Symbols: experimental PS volume fractions profiles for the diffusion experiment conducted at 393 K (Sample B in Table 1). Solid lines: convoluted diffusion model simulations.

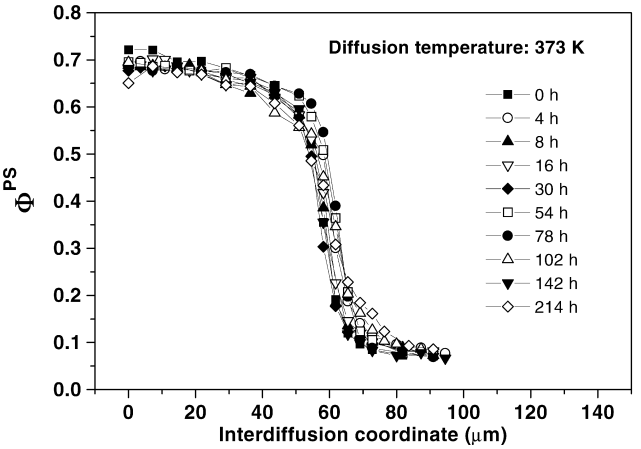

Fig. 6. Experimental PS volume fractions profiles for the diffusion experiment conducted at 373 K (Sample A in Table 1). Measurements were made using the Method B (laser aligned parallel to the diffusion coordinate).

the advancing diffusion front. Fig. 3B shows the diffusion model predictions for the same temperature and times as Fig. 3A, convoluted with the confocal Raman depth resolution curve. The convoluted simulation results coincide almost exactly with the experimental results. The only difference observed between the predictions and the experimental data is the extension of the fictitious tails placed ahead of the diffusion fronts. This difference may well be due to an optimistic prediction of the instrumental depth resolution curve (actual FWHM being larger than predicted), as mentioned in Ref. [20].

Fig. 4 is used to quantitatively compare convoluted diffusion model predictions with experimental data. The experimental points lie almost exactly on the curves corresponding to the model predictions, within experimental error.

Up to now, the parameter most used to follow the time evolution of the diffusion process in limited-supply experiments has been the chemical composition of the plateau region behind the advancing diffusion front [14–16]. The main reason to use this parameter is the difficulties involved in the precise determination and modeling of the tails originated by poor instrumental depth resolutions. Chemical composition at this plateau region is easier to measure, and free from deviations caused by poor instrumental resolution. Therefore, measurements performed using Method A and Method B coincides exactly in this region.

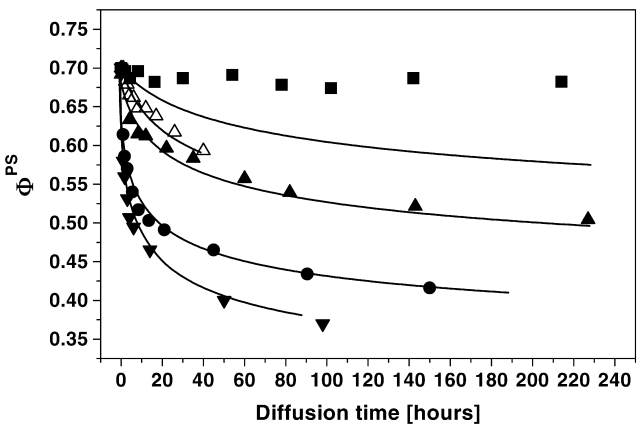

Fig. 5. Time evolution of the PS volume fraction at the plateau region behind the advancing diffusion front. Solid lines: diffusion model predictions. ■: Sample A, ▲: Sample B, △: Sample C, ●: Sample D, ▼: Sample E.

Fig. 5 shows the chemical composition of the plateau region behind the advancing diffusion front—in the form of PS volume fraction—as a function of the diffusion time for all the samples used for this work. The experimental data shown correspond to average values for the outer 20 μm of the PS-rich layer. Continuous lines correspond to the diffusion model predictions. Diffusion temperatures are shown in Table 1. The agreement between experimental data and model predictions is excellent for the complete range of times and temperatures studied, for all temperatures used above 373 K. The same type of plot has been used in Ref. [15] (Figs. 9 and 10), and the data converted to a plot of instantaneous front velocity versus plateau PS volume fraction (Fig. 11). The purpose of this type of plot is to show that—for the experimentally observable plateau PS volume fraction range—the values of the experimentally measured diffusion front instantaneous velocity coincide with the model predictions. Therefore, diffusion control via a Case-II mechanism is clearly ruled out.

The only disagreement found in Fig. 5, between model predictions and experimental data occurs for the experiment conducted at 373 K. The diffusion model predicts advances of the diffusion front which are far more pronounced than the experimental results, when the values of the Flory interaction parameter are taken from Eq. (11). The diffusion slow down has been observed for other authors [26,27] when the diffusion temperature approaches the coexistence curve and has been also linked to unfavorable values of the

Flory thermodynamic interaction parameter. This fact confirms observations published in an earlier work [15]. The values of the Flory thermodynamic interaction parameter at 373 K have been estimated from Eq. (11), and this amounts to an extrapolation from measurements made in the range between 454 and 588 K, published in Ref. [26]. Using higher (less favorable) values for the Flory thermodynamic interaction parameter in the model calculations—as suggested in Ref. [15]—good agreement is found between the experimental results and the model calculations A detailed explanation and a quantitative evaluation of the possible causes for this behavior has been advanced, with an analysis of entropic and enthalpic effects relative influences [15]. This experiment also sheds more light on the diffusion controlling mechanism, as it indicates that the influence of the liquid PS osmotic pressure on the whole process of diffusion front advancing rate is negligible.

In Fig. 6 all the experimental data measured on the same spot of the sample used for the diffusion experiments conducted at 373 K are shown. It can be observed that the advance of the diffusion front after 214 h is almost nil, and the most observable effects are small, monotonic changes in the size of tails of the chemical composition profiles, which seem to confirm earlier published observations on the composition dependence of the relative weights of the entropic and enthalpic terms on the chemical potential gradient [15].

The slight changes of the interphase tails for this diffusion experiment at the longest diffusion times also indicate that the Flory–Huggins interaction parameter may well be the cause for this diffusion slowing down. As already pointed out in Ref. [15], the influence of the Flory–Huggins interaction parameter is highest at intermediate compositions (Φ^{PS} close to 0.5), and becomes close to nil for Φ^{PS} close to 0 or to 1. Therefore, the PS can dissolve all the necessary amount of PPO at the interface (where the value of the thermodynamic factor is maximum) driven by the strong influence of the entropic term. The PPO transport away from the interface is controlled (and slowed down at this temperature) by the diffusion process at intermediate Φ^{PS} values, where the influence of the Flory–Huggins interaction parameter becomes more important. For Φ^{PS} close to 0 or to 1, the influence of the entropic term causes the slight increase in tail sizes, because the dissolution process at the interface and the diffusion at high Φ^{PS} values (low local T_g) become slightly faster than the controlling diffusion step.

5. Conclusions

The diffusion model used predicts accurately the diffusion rates for all species in a broad range of experimental conditions, like temperature, local chemical compositions, local T_g and local molecular weight distribution. Experimental measurements and calculations of composition and temperature dependent monomeric friction factor done by other authors are proven to be very precise. Accurate diffusion rates predictions are obtained for diffusion temperatures that ranged from 393 to 453 K, which are equivalent to a span from 100 to 40 K below the glass transition of the high-T_g layer. For this temperature range and for the experimental setup used, along the diffusion path the local chemical compositions change by a factor of 14, the local T_g values change by 175 K, and the monomeric friction factor changes by a factor higher than 10^{14}. This is a very demanding test for the diffusion model and experimental data used for calculations.

The same diffusion model has been proven correct and accurate for liquid–liquid and liquid–solid diffusion pairs, with the same restrictions and boundary conditions, including Eq. (4) at the interphase region. This fact supports earlier published assumptions [15] for a relatively fast dissolution at the interphase, coupled with a relatively slow diffusion controlled by the same parameters as in the liquid–liquid diffusion. Therefore, the physical diffusion model proposed is experimentally confirmed.

No assumptions are made about the controlling mechanism for the dissolution at the interphase, but the liquid PS penetration into the glassy solid PPO (if any) seems to be much slower than the PPO dissolution. Further experiments, using experimental techniques that may give information on the nanometer scale, may help to elucidate these important details.

The diffusion experiments conducted at 373 K confirm that the liquid–liquid diffusion process is slowed down effectively. The driving force for this diffusion process is the product of the chemical potential gradient times the kinetic factor that depends on the monomeric friction factor. As the monomeric friction factor is not expected to change much going from 393 to 373 K, the diffusion slowing down can be safely assigned to a change of the chemical potential gradient. For the chemical potential gradient, the only temperature dependent parameter is the Flory–Huggins interaction parameter, which is therefore supposed to be the cause for this diffusion slowing down.

Acknowledgements

Financial support from Agencia Nacional de Promoción de Ciencia y Tecnología (ANPCYT-PICT 14-07247) and from Programa de Cooperación con Iberoamérica and CYTED (VIII-11) is acknowledged. J.P. Tomba would also like to thank Laura Izaguirre and David García López (Departamento de Física de la Materia Condensada, Universidad de Valladolid) for their help in the preparation of the diffusion experiments; also Juan Asarou (INTEMA-Universidad Nacional de Mar del Plata) for fine sample holders system design and machining.

References

[1] Mills PJ, Green PF, Palmstron CJ, Mayer JW, Kramer EJ. J Polym Sci, Polym Phys Ed 1986;24:1.
[2] Tomba JP, Carella JM. J Polym Sci, Polym Phys Ed 1999;37:3097.
[3] Vrentras JS, Jarzebski CM, Duda JL. AIChE J 1975;21(5):894.
[4] Thomas NL, Windle AH. Polymer 1982;23:529.
[5] Hui C-Y, Wu K-C, Lasky RC, Kramer EJ. J Appl Phys 1987;61(11): 5129.
[6] Hui C-Y, Wu K-C, Lasky RC, Kramer EJ. J Appl Phys 1987;61(11): 5137.
[7] Lasky RC, Kramer EJ, Hui C-Y. Polymer 1988;29:673.
[8] Gall TP, Lasky RC, Kramer EJ. Polymer 1990;31:1491.
[9] Wu JC, Peppas NA. J Appl Polym Sci 1993;49:1845.
[10] Argon AS, Cohen RE, Patel AC. Polymer 1999;40:6991.
[11] Sauer BB, Walsh DJ. Macromolecules 1991;24:5948.
[12] Composto RJ, Kramer EJ. J Mater Sci 1991;26:2815.
[13] Jabbari E, Peppas NA. Macromolecules 1993;26(9):2175.
[14] Nealey PF, Cohen RE, Argon AS. Polymer 1995;36(19):3687.
[15] Tomba JP, Carella JM, García D, Pastor JM. Macromolecules 2001; 34(7):2277.
[16] Zhou Q-Y, Argon AS, Cohen RE. Polymer 2001;42:613.
[17] Pardo E, Tomba JP, Carella JM. Comput Theor Polym Sci 2000;10(6): 523.
[18] Tomba JP, Carella JM, Pardo E. J Polym Sci, Part B: Polym Phys 1997;35:2435.
[19] Tomba JP, Carella JM, Pastor JM, Fernández MR. Macromol Rapid Commun 1998;19:413.
[20] Everall N. Appl Spectrosc 2000;54(6):773.
[21] Tabaksblat R, Meier RJ, Kip BJ. Appl Spectrosc 1992;46:60.
[22] Tomba JP, Eliçabe G. Submitted for publication.
[23] Tomba JP, De la Puente E, Pastor JM. J Polym Sci, Part B: Polym Phys 2000;38:1013.
[24] Kramer EJ, Green PF, Palmstrom CJ. Polymer 1984;25:473.
[25] Composto RJ, Kramer EJ, White DM. Polymer 1990;31:2320.
[26] Composto RJ, Kramer EJ, White DM. Macromolecules 1988;21: 2580.
[27] Losch A, Woermann D, Klein J. Macromolecules 1994;27:5713.